

Efficient Fractional Order Reference Model of Adaptive Controller Design for Multi-input Multi-output Thermal System

Jutarut Chaoraingern^{a,1}, Vittaya Tipsuwanporn^{a,2}, Arjin Numsomran^{a,3}

^a Department of Instrumentation and Control Engineering, Faculty of Engineering, King Mongkut's Institute of Technology Ladkrabang, Bangkok, 10520, Thailand.

E-mail: ¹61601036@kmitl.ac.th, ²vittaya.ti@kmitl.ac.th, ³arjin.nu@kmitl.ac.th

Abstract— The diverse control techniques have been combined with fractional calculus to enhance the control system performance. This paper presents an efficient fractional-order model reference adaptive controller (FOMRAC) design, which aims to demonstrate the solution for temperature reference tracking and cross-coupling rejection in the multi-input multi-output thermal system as well as cognizing of power consumption saving constraints. The mathematical modeling, nonlinear dynamic characteristic details, and system identification of the thermal system are described while the fractional-order controller combined with a model reference adaptive control (FOMRAC) based on MIT rule is developed so that to create the nonlinear adaptive mechanism which enables the excellent performance to control the multi-input multi-output thermal system. Likewise, a decoupling compensator is constructed to remunerate the effect of the cross-coupling interaction. The validation of the proposed control scheme is performed through the Matlab simulation and the experiment on the multi-input multi-output thermal system. The results illustrated the FOMRAC technique in which the controller's adjustable parameters can provide efficiency stability and performance to minimize the settling time and percent overshoot of the control system response. Besides, the analysis of the power consumption in the control system is addressed to reinforce the useful ability of the proposed method compared with the integral-order model reference adaptive controller (IOMRAC) and the traditional PID controller. The results revealed that the proposed FOMRAC technique exhibited much better than other methods because of the effective optimization of adaptive gain mechanism and fractional-order operators.

Keywords— fractional order controller; model reference adaptive; multi-input multi-output; thermal control system.

I. INTRODUCTION

The fractional calculus has received much attention in the past decade due to providing a great ability to identify the memory and properties of numerous processes [1]-[2]. Likewise, it has been made a practical use in the broad areas of applications such as science, chemistry, electrical engineering, image processing, uncrewed aerial vehicle, and robotics [3]. Also, the fractional calculus has been applied to the control system analysis and design so that improving the performance and robustness of the control system. For example, the fractional-order controller was implemented in a two-wheeled inverted pendulum, while the parameters of the controller were optimized by swarm algorithms to obtain better performance [4]. A study of fractional order PID (FOPID) applied to the induction motors control was proposed for illustrating the impact of vibration and noise reduction [5]. The design techniques of FOPID controller for the motor and generator control system was described by investigating the performance and robustness against the external-disturbances [6], [7]. The FOPID designed by chaotic atom search optimization (ChASO) algorithm was

presented to describe the optimal parameters for motor speed control [8]. The FOPID controller designed by a dynamic particle swarm optimization method was implemented in the magnetic levitation system [9]. The fractional-order controls were used for improving the efficiency and robust reliability of the robotic manipulator tracking control toward the external disturbances [10], [11].

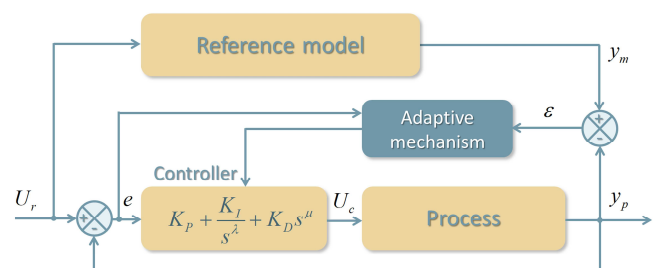


Fig. 1 A FOMRAC block diagram

Many control techniques have been integrated with fractional order control to enhance the control system performance or increase the robustness against the

disturbance and parameter uncertainty. For instance, the fractional-order sliding mode control was implemented in a pneumatic system to enable better position tracking accuracy [12]. The fractional-order fuzzy PID control was performed to show better results over the integer order-PID and fuzzy-PID controller when applied to the wind power hybrid device [13]. The fractional-order fuzzy PID was applied to the wind turbine pitch control for improving performance and robustness [14]. The type-2 fractional order fuzzy PID controller was suggested by a design algorithm, such as hybrid firefly algorithm-particle swarm optimization for improving the system response and stability [15], [16]. The fractional-order fuzzy sliding mode control was deployed to the simulation of a tethered satellite system (TSS) for decreasing settling time and overshoot of the tether response [17].

In the case of adaptive control, several studies have been investigated a combination of fractional calculus and adaptive mechanism. For example, the model-free adaptive fractional-order control was proposed for illustrating the online tuning technique suitable for linear time-varying systems [18]. The adaptive fractional-order sliding mode control was applied to a micro gyroscope for achieving trajectory tracking control [19], [20]. The adaptive fractional-order combined with sliding mode control and super twisting sliding mode control was implemented in motor speed control for increasing speed tracking precision and robustness to process uncertainties [21]-[22]. The adaptive fractional-order sliding mode control was applied to the application of trajectory tracking of quadrotor for reducing the effect of wind disturbance and load variations [23]. Adaptive fractional fuzzy sliding mode control was explained to address the strategy of permanent magnet synchronous motor motion control [24]-[25]. The adaptive interval type-2 fuzzy fractional-order backstepping sliding mode control was presented in [26] for demonstrating the solution of perturbation rejection for a nonlinear system.

As the aforementioned aspect, much work on the potential of fractional order control techniques has been carried out. However, there are still some critical issues for an implement to multi-input multi-output (MIMO) thermal system. The main contribution of this paper is to propose an efficient fractional-order model reference adaptive controller (FOMRAC) design for the multi-input multi-output thermal system. In this study, we focus on designing the effective nonlinear adaptive control mechanism combined with the fractional-order controller, which aims to demonstrate the solution for temperature reference tracking and cross-coupling rejection in the multi-input multi-output thermal system as well as cognizing of power consumption saving constraints. The mathematical modelling, nonlinear dynamic characteristic details, and system identification of the thermal system are described while the fractional-order controller combined with a model reference adaptive control (FOMRAC) based on MIT rule is developed so that to create the nonlinear adaptive mechanism which enables the excellent performance to control the multi-input multi-output thermal system. Likewise, a decoupling compensator is constructed to remunerate the effect of the cross-coupling interaction. The validation of the proposed control scheme is performed through the Matlab simulation and the experiment

on the multi-input multi-output thermal system. In addition, the analysis of the power consumption in the control system is demonstrated to reinforce the effective ability of the proposed method compared with the integral-order model reference adaptive controller (IOMRAC) and the traditional PID controller. The paper is organized as follows: the materials and methods are explained in section II. The result and discussion are demonstrated in section III, while the conclusions are addressed in section IV.

II. MATERIALS AND METHODS

A. Fractional Order Model Reference Adaptive Controller (FOMRAC)

In the following paragraphs, we describe the proposed control methodologies of FOMRAC combined with a decoupling compensator. The structure of the control system in Fig. 1, comprises three major components. The first part is a fractional-order PID control, the feedback loop of the thermal system; the second part is a model reference adaptive control (MRAC), the adjustment mechanism based on MIT rule supporting for a nonlinear control algorithm; the third part is decoupling compensator deployed for diminishing the cross-coupling in the MIMO system. The controller gains are adaptable using the MRAC mechanism based on MIT rule. Likewise, the appropriate values of fractional-order operators (λ, μ) are defined by Integral Square Error (ISE) tuning method and the power consumption constraints.

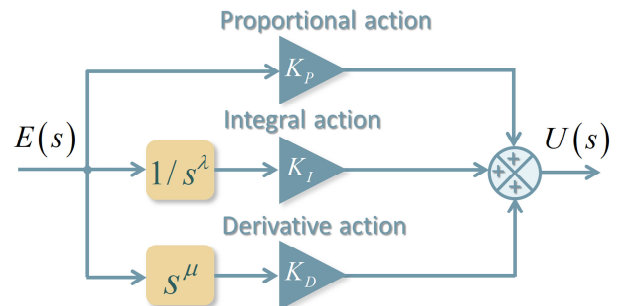


Fig. 2 A block diagram of the FOPID control

1) *Fractional Order PID*: Considering a definition of fractional derivative denoted by Grunwald–Letnikov [27] in Eq. 1, it is widely applied to the implementation of fractional-order control system design.

$$\begin{aligned} {}_a D_t^q f(t) &= \frac{d^q f(t)}{d(t-a)^q} \\ &= \lim_{h \rightarrow 0} \frac{1}{h^q} \sum_{i=0}^{\lfloor (t-a)/h \rfloor} (-1)^i \binom{q}{i} f(t-ih) \end{aligned} \quad (1)$$

where D is the mathematical operator. q is the fractional-order operation. a and t are limit ranges. h is the small step size. $\binom{q}{i}$ is the function of $\frac{(q)(q-1)(q-2)\dots(q-i+1)}{\Gamma(i-1)}$.

The basic block diagram of FOPID controller in Fig. 2. consists of the block of proportional gain (K_p), integral gain (K_I), derivative gain (K_D), as well as differentiation

and integration operator with fractional-order (μ, λ) respectively. The main benefit of this approach is that the five parameters $(K_p, K_I, K_D, \lambda, \mu)$ enhance control ability, which enables adjustment of the performance indexes. The function of the FOPID controller transfer function is defined as follows.

$$G_{FOPID}(s) = K_p + K_I \frac{1}{s^\lambda} + K_D s^\mu, \quad (\lambda, \mu > 0) \quad (2)$$

where K_p, K_I, K_D are the PID gains. λ and μ are fractional operators.

2) *Model reference adaptive control*: Fig. 3 demonstrates the details of the adaptive mechanism in FOMRAC, which is employed for automatically adjusting the FOPID controller gains. The reference model block is designed from a mathematical model of the system having an appropriate response to provide the output reference signal (y_m) for comparing with the output of the process (y_p) . The deviation between y_p and y_m defined as the error signal is entered into the adjustment mechanism to achieve the optimal values of controller parameters that enhance the performance of the control system.

In this research, the adjustment mechanism is developed using MIT adaptive rule [28], which implements the algorithms in the following descriptions.

- The error signal ε

$$\varepsilon = y_p - y_m \quad (3)$$

- The square error function $J(\theta)$

$$J(\theta) = \frac{1}{2} \varepsilon^2(\theta) \quad (4)$$

- The changing rate of θ

$$\frac{d\theta}{dt} = -\gamma \frac{\partial J}{\partial \theta} = -\gamma \varepsilon \frac{\partial \varepsilon}{\partial \theta} \quad (5)$$

where $\frac{\partial J}{\partial \theta}$ is the function of square error with respect to θ .

θ refers to the controller parameter. γ is an adaptation gain. ε refers to the error signal, which is the differentiate between the reference model response y_m and the process response y_p .

The transfer function of the reference model $G_{ref}(s)$ is designed by the pole placement method characterized by settling time and percent of maximum overshoot specification.

$$G_{ref}(s) = \frac{Y_m(s)}{U_c(s)} = \frac{b_m s^m + b_{m-1} s^{m-1} + \dots + b_1 s + b_0}{a_m s^n + a_{m-1} s^{n-1} + \dots + a_1 s + a_0} \quad (6)$$

where Y_m is the output of the reference model. U_c is the control signal. $b_m \square b_0$ and $a_m \square a_0$ are coefficients of reference model transfer function.

The process transfer function $G_p(s)$ is defined as

$$G_p(s) = \frac{N_p(s)}{D_p(s)} = \frac{b_p s^v + b_{p-1} s^{v-1} + \dots + b_1 s + b_0}{a_p s^u + a_{p-1} s^{u-1} + \dots + a_1 s + a_0} \quad (7)$$

where $N_p(s), D_p(s)$ refer to the numerator and denominator polynomial of the process transfer function, respectively. $b_p \square b_0$ and $a_p \square a_0$ refer to the coefficients of the process transfer function.

The FOMRAC transfer function is expressed as

$$G_{FOMRAC}(s) = K_p + K_I \frac{1}{s^\lambda} + K_D s^\mu, \quad (\lambda, \mu > 0) \quad (8)$$

where K_p, K_I, K_D are defined as the gain of PID controller. λ, μ refer to the fractional operators.

The main merits of MIT gradient rule are the simplicity and usefulness in calculating the controller parameter values, which increase the capability of the controller. Referring to MRAC adjustment mechanism using MIT adaptive control rule, the PID controller gains are calculated as

$$K_p = -\gamma_p s \frac{\varepsilon N_p(s)}{s B(s)} y_p \quad (9)$$

$$K_I = -\gamma_i \frac{\varepsilon N_p(s)}{s B(s)} [U_c - y_p] \quad (10)$$

$$K_D = -\gamma_d s^2 \frac{\varepsilon N_p(s)}{s B(s)} y_p \quad (11)$$

where γ refers to the adaptation gain of controller parameters. y_p refers to the process output signal. U_c is defined as the controller signal.

3) *Decoupling Compensator*: Generally, the MIMO thermal system has controllability disadvantage of disturbance between inputs and outputs and the presence of heat convection and radiation between 2 heaters. Therefore the decoupling compensators are applied to minimize cross-coupling between two interaction systems [29].

In reference to the thermal system transfer matrix $(g_{11}, g_{12}, g_{21}, g_{22})$, the decoupling compensators are defined as

$$G_{decouple}(s) = \begin{bmatrix} 1 & -D_{12}(s) \\ -D_{21}(s) & 1 \end{bmatrix} \quad (12)$$

$$D_1(s) = \frac{g_{21}(s)}{g_{22}(s)} \quad (13)$$

$$D_2(s) = \frac{g_{12}(s)}{g_{11}(s)} \quad (14)$$

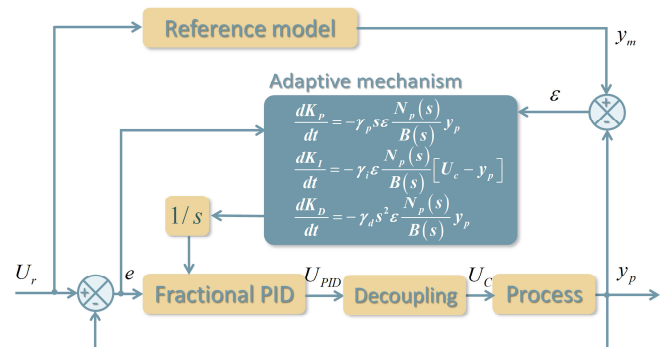


Fig. 3 A block diagram of FOMRAC for MIMO thermal system

Therefore, the compensated models of the MIMO thermal system (g_{11c}, g_{22c}) are expressed as

$$G_{p_comp}(s) = \begin{bmatrix} g_{11c}(s) & 0 \\ 0 & g_{22c}(s) \end{bmatrix} \quad (15)$$

$$g_{11c}(s) = G_{11}(s) - D_1(s)G_{12}(s) \quad (16)$$

$$g_{22c}(s) = G_{22}(s) - D_2(s)G_{21}(s) \quad (17)$$

B. Multi-input Multi-output Thermal System

The MIMO thermal systems are attracting widespread discussions due to the needs of design and optimization implemented in various applications such as manufacturing, materials processing, energy conversion, and power generation. Their nonlinear characteristic, interaction, and parameter perturbation are challenging control problem which needs advanced control techniques.

1) *Hardware*: Fig. 4 depicts a small-scale thermal system that is used for the practical implementation of MIMO thermal process control analysis and design [30]. It consists of an Arduino shield combined with Arduino UNO microcontroller board based on the ATmega328P, 5V power supply, and a USB communication cable. The thermal system is a multivariable system composed of 2 heaters and 2 temperature sensors. The interaction between the heater/sensor pairs is occurred by thermal convection and radiation to the temperature sensor. Thus, it enables to imply cross-coupling between heater 1 and heater 2 so that the thermal system is sufficient to demonstrate the evaluation of multivariable control strategies.



Fig. 4 Multi-input multi-output thermal system

2) *Mathematical Model*: A mathematical model is derived for understanding the behavior of MIMO thermal system, which is governed by nonlinear characteristics, interaction disturbances, and parameter perturbation. The objective is to control the temperature of the thermal systems through two heaters. Thermal energy (Q_1, Q_2) is the process inputs, and the outputs are temperature in thermal systems (T_i). The nonlinear plant equations, defining the temperature characteristics in each thermal system, are derived from energy balances of thermal convection and radiation as follows [31].

• Non-Linear Model

$$mc_p \frac{dT_1}{dt} = UA(T_a - T_1) + \varepsilon_i \sigma A (T_a^4 - T_1^4) + UA_s (T_2 - T_1) + \varepsilon_i \sigma A_s (T_2^4 - T_1^4) + \alpha_1 Q_1 \quad (18)$$

$$mc_p \frac{dT_2}{dt} = UA(T_a - T_2) + \varepsilon_i \sigma A (T_a^4 - T_2^4) + UA_s (T_1 - T_2) + \varepsilon_i \sigma A_s (T_1^4 - T_2^4) + \alpha_2 Q_2 \quad (19)$$

• Linear Model

$$\tau_{12} \frac{dT_1}{dt} = [T_a - T_1] + K_3 [T_2 - T_1] + K_1 Q_1 \quad (20)$$

$$\tau_{12} \frac{dT_2}{dt} = [T_a - T_2] - K_3 [T_2 - T_1] + K_2 Q_2 \quad (21)$$

where

$$\tau_{12} = \frac{mc_p}{(UA + \varepsilon_i \sigma A 4T_{a0}^3)}$$

$$K_1 = \frac{\alpha_1}{(UA + \varepsilon_i \sigma A 4T_{a0}^3)}$$

$$K_2 = \frac{\alpha_2}{(UA + \varepsilon_i \sigma A 4T_{a0}^3)}$$

$$K_3 = \frac{(UA_s + \varepsilon_i \sigma A_s 4T_{a0}^3)}{(UA + \varepsilon_i \sigma A 4T_{a0}^3)}$$

m is mass. C_p is heat capacity. T_i is temperature. T_a is ambient temperature. T_0 is initial temperature. U is heat transfer coefficient. A is surface area. A_s is gap area. α_i is heater factor. ε_i is emissivity. σ is Stefan Boltzmann constant. Q is heater input.

• Linearized State equation

$$\begin{bmatrix} dT_1 \\ dT_2 \end{bmatrix} = \begin{bmatrix} -\left(\frac{1+K_3}{\tau_{12}}\right) & \frac{K_3}{\tau_{12}} \\ \frac{K_3}{\tau_{12}} & -\left(\frac{1+K_3}{\tau_{12}}\right) \end{bmatrix} \begin{bmatrix} T_1 \\ T_2 \end{bmatrix} + \begin{bmatrix} \frac{K_1}{\tau_{12}} & 0 \\ 0 & \frac{K_2}{\tau_{12}} \end{bmatrix} \begin{bmatrix} Q_1 \\ Q_2 \end{bmatrix} + \begin{bmatrix} \frac{1}{\tau_{12}} \\ \frac{1}{\tau_{12}} \end{bmatrix} T_a \quad (22)$$

$$\begin{bmatrix} y_1 \\ y_2 \end{bmatrix} = \begin{bmatrix} 1 & 0 \\ 0 & 1 \end{bmatrix} \begin{bmatrix} T_1 \\ T_2 \end{bmatrix} \quad (23)$$

where

$$x = \begin{bmatrix} T_1 \\ T_2 \end{bmatrix} = \text{state variables}$$

$$y = \begin{bmatrix} T_1 \\ T_2 \end{bmatrix} = \text{output variables}$$

$$u = \begin{bmatrix} Q_1 \\ Q_2 \\ T_a \end{bmatrix} = \text{input variables}$$

• Transfer Matrix

$$G(s) = C(sI - A)^{-1} B, \begin{bmatrix} Y_1(s) \\ Y_2(s) \end{bmatrix} \quad (24)$$

$$= \begin{bmatrix} g_{11}(s) & g_{12}(s) \\ g_{21}(s) & g_{22}(s) \end{bmatrix} \begin{bmatrix} U_1(s) \\ U_2(s) \end{bmatrix} \quad (25)$$

$$g_{11} = \frac{T_1(s)}{Q_1(s)} = \frac{K_1(\tau_{12}s + 1 + K_3)}{(\tau_{12}s + 1 + K_3)^2 - K_3^2} \quad (25)$$

$$g_{12} = \frac{T_1(s)}{Q_2(s)} = \frac{K_2 K_3}{(\tau_{12}s + 1 + K_3)^2 - K_3^2} \quad (26)$$

$$g_{21} = \frac{T_2(s)}{Q_1(s)} = \frac{K_1 K_3}{(\tau_{12}s + 1 + K_3)^2 - K_3^2} \quad (27)$$

$$g_{22} = \frac{T_2(s)}{Q_2(s)} = \frac{K_2(\tau_{12}s + 1 + K_3)}{(\tau_{12}s + 1 + K_3)^2 - K_3^2} \quad (28)$$

3) *System Identification*: Fig. 5 demonstrates the MIMO thermal curve fitting system identification. The results from the sum of squared estimated error (SSE) at 5.3285 provide the model parameters as indicated in Table I.

Referring to the linearized model in Eq. (20)-(21), and the process parameters in Table I, the transfer matrix of the thermal system is demonstrated as.

$$G_{process}(s) = \begin{bmatrix} g_{11}(s) & g_{12}(s) \\ g_{21}(s) & g_{22}(s) \end{bmatrix} \quad (29)$$

$$g_{11}(s) = \frac{2.29e5s^4 + 6.18e4s^3 + 6.04e3s^2 + 2.48e2s + 3.46}{6.66e6s^5 + 2.33e6s^4 + 3.02e5s^3 + 1.77e4s^2 + 4.54e2s + 3.84} \quad (30)$$

$$g_{12}(s) = \frac{1.45e4s^3 + 3.22e3s^2 + 2.23e2s + 4.66}{8.31e6s^5 + 3.22e6s^4 + 4.67e5s^3 + 3.14e4s^2 + 9.62e2s + 10.8} \quad (31)$$

$$g_{21}(s) = \frac{3.38e2s^2 + 47.8s + 1.3}{1.76e5s^4 + 5.45e4s^3 + 5.71e3s^2 + 2.31e2s + 3.1} \quad (32)$$

$$g_{22}(s) = \frac{1.53e6s^5 + 5.81e5s^4 + 8.67e4s^3 + 6.33e3s^2 + 2.25e2s + 3.07}{4.4e7s^6 + 2.06e7s^5 + 3.84e6s^4 + 3.65e5s^3 + 1.84e4s^2 + 4.66e2s + 4.58} \quad (33)$$

TABLE I
PROCESS PARAMETERS OF MIMO THERMAL SYSTEM

Process parameters	Value
Initial temperature (T_0)	30° C
Ambient temperature (T_a)	30° C
Heater Input (Q)	0 to 1 W
Heater factor (α_1)	0.005 W / %Q
Heater factor (α_2)	0.002 W / %Q

Heat capacity (C_p)	500 J / kg · K
Surface area (A)	10 cm ²
Gap area (A_g)	2 cm ²
Mass (m)	0.004 kg
Overall heat transfer coefficient (U)	4.1365 W / m ² · K
Stefan Boltzmann Constant (σ)	5.67x10 ⁻⁸ W / m ² · K ⁴

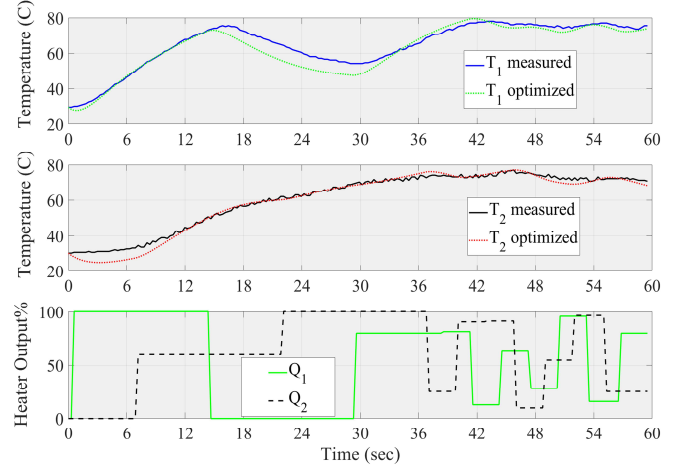


Fig. 5 Process parameters identification for MIMO thermal system: Final SSE objective: 5.3285

III. RESULTS AND DISCUSSION

In this part, for indicating the usefulness of the proposed control strategy, the simulations and experiments are carried out on the multi-input multi-output thermal system. It is compared with the conventional control scheme such as integer-order model reference adaptive control (IOMRAC) as well as integer-order non-adaptive PID.

A. Decoupling Compensator Design

Regarding the decoupling compensator design method mentioned in section II and the linearized system model in Eq. (29) – (33), the decoupling compensators are determined as

$$G_{decouple}(s) = \begin{bmatrix} I & -D_{12}(s) \\ -D_{21}(s) & I \end{bmatrix} \quad (34)$$

$$D_{12}(s) = \frac{2.77e8s^6 + 1.12e8s^5 + 1.78e7s^4 + 1.38e6s^3 + 5.53e4s^2 + 1.06e3s + 7.52}{5.47e9s^7 + 2.68e9s^6 + 5.4e8s^5 + 5.73e7s^4 + 3.47e6s^3 + 1.19e5s^2 + 2.14e3s + 15.7} \quad (35)$$

$$D_{21}(s) = \frac{3.18e7s^6 + 1.43e7s^5 + 2.54e6s^4 + 2.23e5s^3 + 1.02e4s^2 + 2.31e2s + 2.04}{5.78e8s^7 + 3.07e8s^6 + 6.71e7s^5 + 7.82e6s^4 + 5.22e5s^3 + 1.99e4s^2 + 3.98e2s + 3.25} \quad (36)$$

Hence, the compensated model of the MIMO thermal system (g_{11c}, g_{22c}) is expressed as

$$G_{p_comp}(s) = \begin{bmatrix} g_{11c}(s) & 0 \\ 0 & g_{22c}(s) \end{bmatrix} \quad (37)$$

$$g_{11c}(s) = \frac{1.33e15s^{12} + 1.71e15s^{11} + 4.58e14s^{10} + 1.06e14s^9 + 1.59e13s^8 + 1.65e12s^7 + 1.2e11s^6 + 6.27e9s^5 + 2.31e8s^4 + 5.91e6s^3 + 1.0e5s^2 + 1.01e3s + 4.66}{3.86e16s^{13} + 3.71e16s^{12} + 1.6e16s^{11} + 4.14e15s^{10} + 7.08e14s^9 + 8.48e13s^8 + 7.29e12s^7 + 4.56e11s^6 + 2.07e10s^5 + 6.71e8s^4 + 1.51e7s^3 + 2.23e5s^2 + 1.93e3s + 7.39} \quad (38)$$

$$g_{22c}(s) = \frac{7.79e14s^{12} + 6.86e14s^{11} + 2.69e14s^{10} + 6.19e13s^9 + 9.33e12s^8 + 9.67e11s^7 + 7.07e10s^6 + 3.68e9s^5 + 1.36e8s^4 + 3.47e6s^3 + 5.87e4s^2 + 5.93e2s + 2.73}{2.24e16s^{13} + 2.17e16s^{12} + 9.46e15s^{11} + 2.46e15s^{10} + 4.25e14s^9 + 5.14e13s^8 + 4.48e12s^7 + 2.84e11s^6 + 1.31e10s^5 + 4.36e8s^4 + 1.01e7s^3 + 1.56e5s^2 + 1.42e3s + 5.83} \quad (39)$$

B. Fractional-order Model Reference Adaptive Controller Design

Regarding the design of FOMRAC referenced in section II, the response specification of the control system that conforms with the overshoot percentage (PO) is less than 8 percent, and the settling time is less than 300 sec.

$$\text{Model ref1} = \frac{Y_{m1}(s)}{U_1(s)} = \frac{0.0001s^2 + 0.0204s + 0.0008}{s^2 + 0.0347s + 0.0007} \quad (40)$$

$$\text{Model ref2} = \frac{Y_{m2}(s)}{U_2(s)} = \frac{0.0001s^2 + 0.0201s + 0.0007}{s^2 + 0.0312s + 0.0007} \quad (41)$$

The adaptation gains (γ) are defined as Eq (42) and (43) by the MIT adaptive control rule mentioned in section II A-2 to reduce the square error rate, power consumption as well as to achieve the input signal tracking capabilities effectively.

- MRAC adaptation gains 1: $\gamma_{p1} = -1.0 \times 10^{-5}, \gamma_{i1} = -1.0 \times 10^{-9}, \gamma_{d1} = -1.0 \times 10^{-5} \quad (42)$

- MRAC adaptation gains 2: $\gamma_{p2} = -1.0 \times 10^{-5}, \gamma_{i2} = -1.0 \times 10^{-9}, \gamma_{d2} = -1.0 \times 10^{-5} \quad (43)$

The fractional-order controller design can perform the integral square error (ISE) optimization suggested in [32]. Fig. 6 illustrated the appropriate values of fractional operators (λ, μ) which have been found in the range of $\lambda = [0.80; 1.20]$ and $\mu = [0.30; 0.60]$. We, therefore, chose the values as the corresponding controller transfer functions.

$$G_{FOMRAC_1}(s) = K_{p1} + K_{i1} \frac{1}{s^{1.12}} + K_{d1} s^{0.42} \quad (44)$$

$$G_{FOMRAC_2}(s) = K_{p2} + K_{i2} \frac{1}{s^{1.14}} + K_{d2} s^{0.45} \quad (45)$$

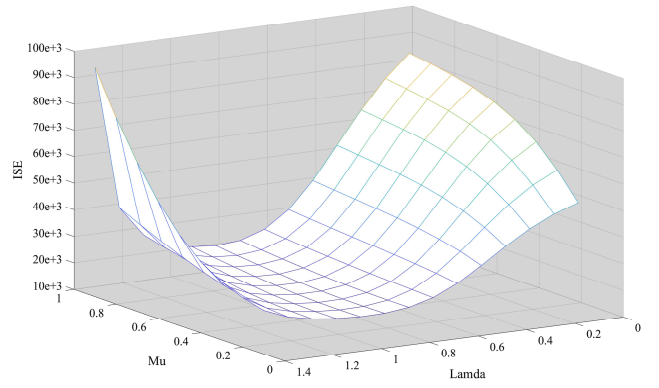


Fig. 6 ISE minimization for fractional order integration (λ) and differentiation operators (μ)

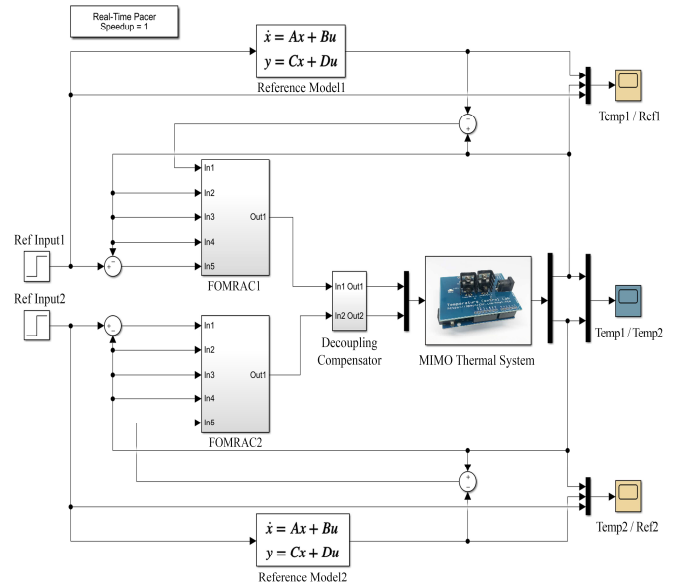


Fig. 7 Simulation program for MIMO thermal system

C. Simulation Result and discussion

This section describes the results of simulation gathered from the Simulink program in Fig. 7 for a nonlinear dynamic model of the MIMO thermal system controlled by the proposed FOMRAC controller completed with the decoupling compensator comparing with IOMRAC and PID control. The target is to control the temperature in thermal system 1 and thermal system 2 to track the step input signal at 50 degrees Celsius using heater input signals (Q_1, Q_2).

Referring to the proposed technique, Fig. 8 illustrates the control system step responses, which use FOMRAC with decoupling compensators. The results of simulation revealed that FOMRAC has better transient responses of a maximum percent overshoot and a settling time over IOMRAC. It is because of the additional fractional-operators that can help the control system to improve control efficiency to minimize maximum percent overshoot, a settling time, ISE, ITAE as mention in Table II.

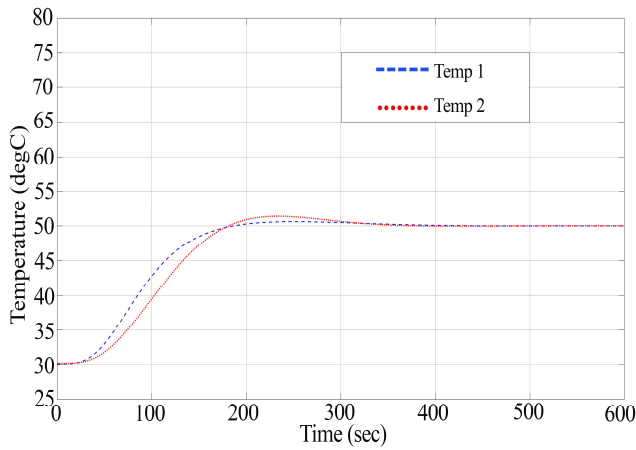


Fig. 8 FOMRAC control step responses

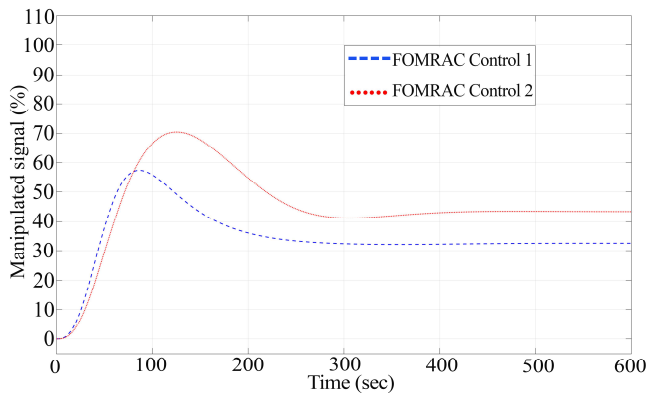


Fig. 9 FOMRAC control manipulated signals

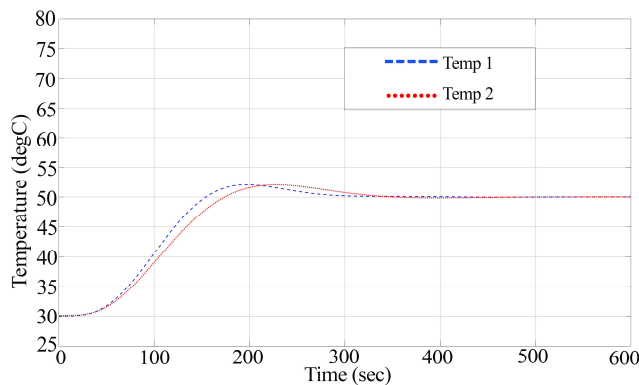


Fig. 10 IOMRAC control step responses

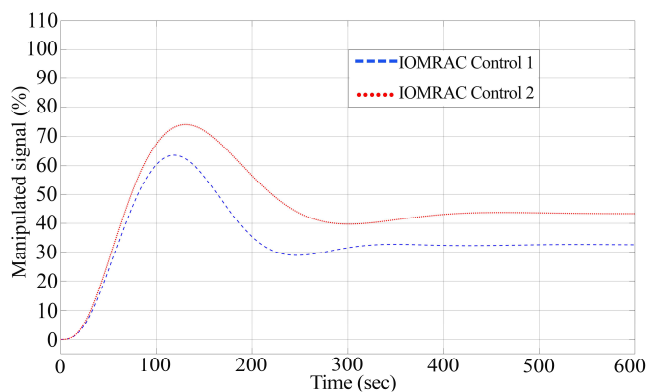


Fig. 11 IOMRAC control manipulated signals

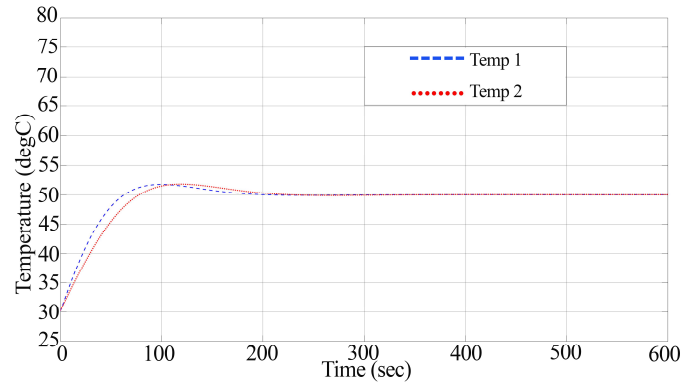


Fig. 12 PID control step responses

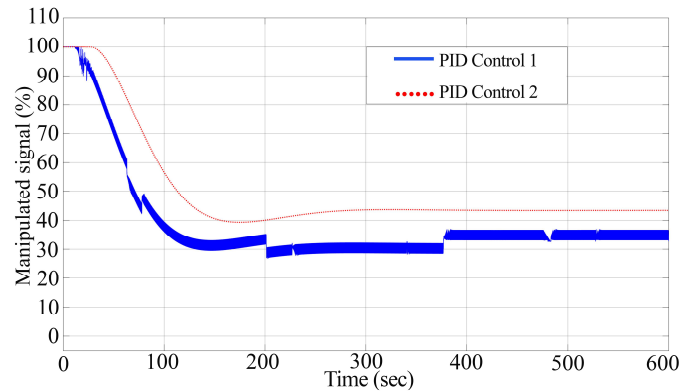


Fig. 13 PID control manipulated signals

TABLE II
SIMULATION PERFORMANCE RESULT COMPARISON

Performance Index	Control Techniques		
	PID	IOMRAC	FOMRAC
Max overshoot (%)	3.58, 3.68	4.08, 4.06	1.2, 2.8
Settling time (sec)	141, 166	288, 288	160, 275
ISE system 1	6.188×10^3	3.126×10^4	2.221×10^4
ISE system 2	8.04×10^3	3.348×10^4	2.451×10^4
ITAE system 1	2.604×10^4	1.441×10^5	1.177×10^5
ITAE system 2	3.781×10^4	1.778×10^5	1.498×10^5
Total Energy Q_1 (W)	114.5	113.5	103.5
Total Energy Q_2 (W)	60.2	59	54

Due to the adaptive gains and the reference model of the FOMRAC mechanism, they provided the slow response of step response so that decreased maximum overshoot and output fluctuation. For this reason, the simulation results of FOMRAC have a lower percentage of maximum overshoot than the traditional PID control while getting more settling time, ISE, ITAE.

Regarding the concern about the total energy consumption which is experientially regarded to be proportional to the integration of energy input signals (Q_1, Q_2), the parameters of controllers and compensators have been optimized depending on the value of the adaptive gains and fractional-order operators for providing an optimal balance of the performance indices such as settling time, percent overshoot, error steady-state, and the controller signal. The result in Fig. 9 illustrates the control signals of FOMRAC case compared with the results from IOMRAC and traditional PID control in Fig. 11, Fig. 13, respectively. As demonstrated in Table II,

FOMRAC with proper parameter optimization required less energy consumption than all other control techniques.

D. Experimental Result and Discussion

This section presents the results obtained from the experimental program in Fig.7, which is generated by Matlab Simulink with Arduino support package. In these experiments, the control algorithm was executed on the host computer real-time communicated between Simulink and the TC-Lab kit over a serial port. The proposed program is divided into 3 main parts as FOMRAC algorithm, the reference model, and the decoupling compensator. The aim is to control the temperature of systems 1 and 2 in order to track the step input signal at 50°C using heater input signals (Q_1, Q_2) .

As regards the proposed FOMRAC technique, Fig. 14 exhibits the step responses of the controlled system using FOMRAC with decoupling compensators. The experimental results revealed that FOMRAC has a better percent overshoot and settling time over other methods. As stated in section II, the proposed FOMRAC with decoupling compensators used temperature outputs (y_1, y_2) and the deviation signals between the reference outputs (y_{m1}, y_{m2}) and temperature outputs (y_1, y_2) for determining the controller gain (K_p, K_I, K_D) dynamically. In addition, the fractional-order of the operations (λ, μ) can help the control system to improve control efficiency. The effectiveness of the proposed approach applied to the MIMO thermal system can be shown that the maximum overshoot of the step responses are 5.3 and 7.2 percent, the setting times are 185 and 233 seconds for $Temp_1$ (blue line) and $Temp_2$ (red line) respectively, while steady- error values are negligible.

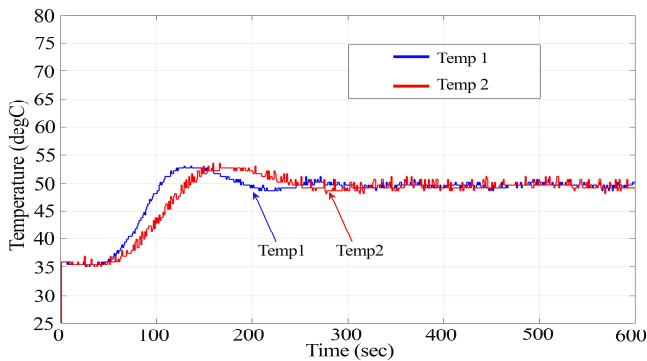


Fig. 14 FOMRAC control step responses

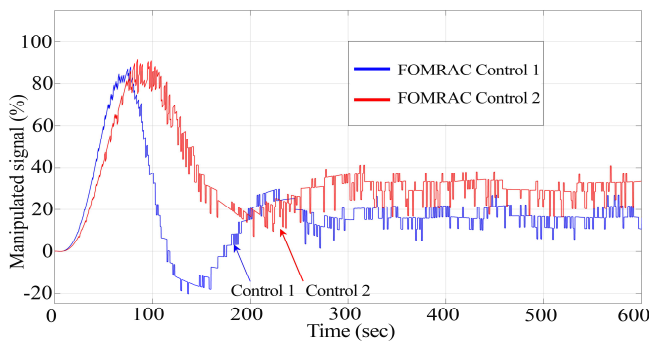


Fig. 15 FOMRAC control manipulated signals

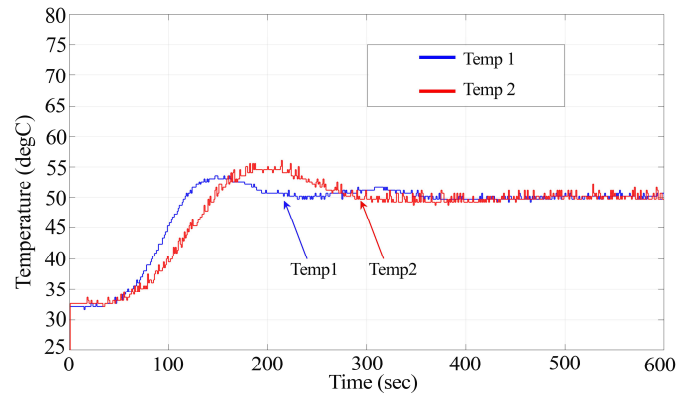


Fig. 16 IOMRAC control step responses

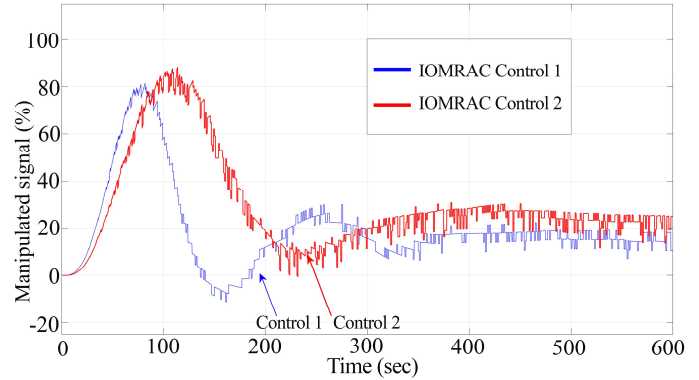


Fig. 17 IOMRAC control manipulated signals

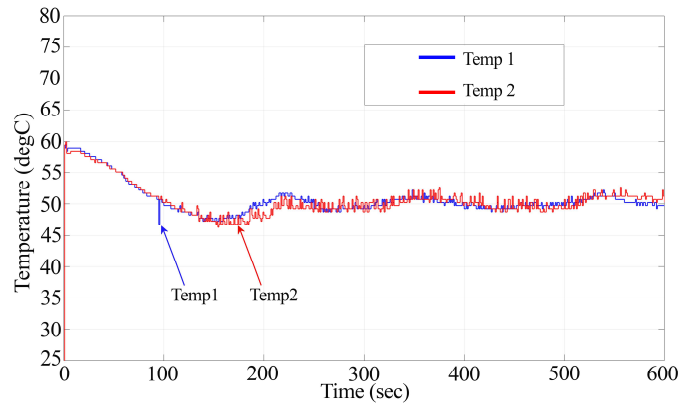


Fig. 18 PID control step responses

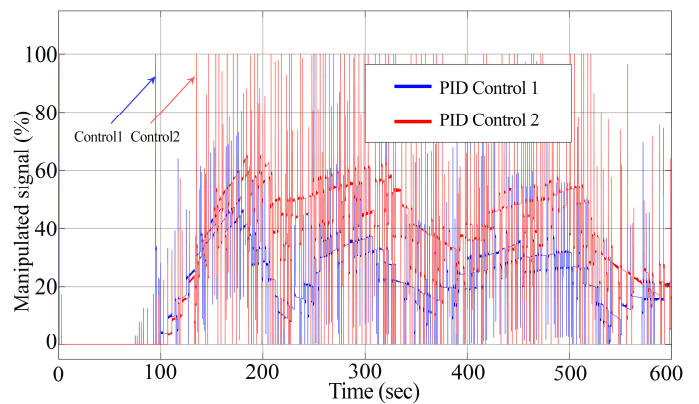


Fig. 19 PID control manipulated signals

TABLE III
EXPERIMENTAL PERFORMANCE RESULT COMPARISON

Performance Index	Control Techniques		
	PID	IOMRAC	FOMRAC
Max overshoot (%)	18.9, 19.9	7.2, 12.1	5.3, 7.2
Settling time (sec)	245, 277	203, 272	185, 233
ISE system 1	1.837×10^4	2.452×10^4	1.558×10^4
ISE system 2	1.884×10^4	2.896×10^4	1.752×10^4
ITAE system 1	2.074×10^5	1.736×10^5	1.32×10^5
ITAE system 2	2.108×10^5	2.735×10^5	2.01×10^5
Total Energy Q_1 (W)	104	73	62
Total Energy Q_2 (W)	39.4	37.6	33.8

Furthermore, the output response of FOMRAC control provided the lowest error performance indexes of ISE and ITAE, as described in Table III. Nevertheless, Fig. 15 presents the control signals of FOMRAC case compared with the cases of IOMRAC and traditional PID in Fig. 17, Fig. 19 respectively. It is apparent in Table III that the total energy consumption for the FOMRAC controllers is 62W and 33.8W, while IOMRAC required more at 73W and 37.6W. Nevertheless, the traditional PID control expressed a saturated conditional of the control signal as well as demanded more heater energy at 104W and 39.4W.

In summary, the simulation and experimental results demonstrated that the proposed technique FOMRAC with the decoupling compensator exhibited an excellent performance to control the MIMO thermal system. The advantage of the proposed technique over IOMRAC and traditional PID controller demonstrated in Table II and III. The results indicated clearly that the IOMRAC model had restricted the changes of the response while FOMRAC, which minimized the settling time and percent overshoot by changing the fractional-order of the operation (λ, μ). In the case of PID control, they performed fewer performances expressed by the experimental results having large overshoot in transient response and oscillations in steady-state and the saturated conditional of control signal due to non-adaptive control ability. By the total energy optimization, the proposed FOMRAC technique exhibited much better than other methods because of the effective optimization of adaptive gain mechanism and fractional-order operators.

IV. CONCLUSIONS

In this paper, the fractional-order model reference adaptive controller (FOMRAC) is presented. The proposed controller design scheme is applied to the multi-input multi-output thermal system for achieving the performance of the control system, reducing the cross-coupling disturbance as well as cognizing of power consumption saving constraints. The nonlinear mathematical modelling and system identification of a thermal system is described. At the same time, the fractional-order controller combined with a model reference adaptive control based on MIT rule and decoupling compensator is constructed. The validations of the proposed control scheme are performed through the Matlab simulation as well as the experiment on the multi-input multi-output thermal system. Results demonstrated significantly that the proposed control technique provided sufficient efficiency

and stability effectiveness compared with the integer-order model reference adaptive control (IOMRAC) and traditional PID control. Further analysis showed that the proposed FOMRAC technique with proper parameter optimization reinforces the usefulness for energy consumption saving over other control schemes. Future work will concentrate on implementing the FOMRAC algorithm in the STM32F4 embedded system for extending the control and application capacity of a multi-input multi-output thermal control system.

NOMENCLATURE

D	mathematical operator	
K_P	proportional gain	
K_I	integral gain	
K_D	derivative gain	
ISE	integral square error	
ITAE	integral time absolute error	
ε	error signal	
y_p	output of the process	
y_m	output reference signal	
γ	adaptation gain	
G_{ref}	reference model transfer function	
G_p	process transfer function	
G_{fopid}	FOPID controller transfer function	
G_{fomrac}	FOMRAC controller transfer function	
$G_{decouple}$	decoupling compensator transfer function	
G_{p_comp}	compensated process transfer function	
Q_i	thermal energy input	W
T_i	temperature in thermal systems	$^{\circ}\text{C}$
T_a	ambient temperature	$^{\circ}\text{C}$
T_0	initial temperature	$^{\circ}\text{C}$
A	surface area	cm^2
A_s	gap area	cm^2
m	mass	kg
C_p	heat capacity	J / kg · K
α_i	heater factor	W / % Q
σ	Stefan Boltzmann constant	W / $\text{m}^2 \cdot \text{K}^4$

REFERENCES

- [1] J. Sabatier, P. Lanusse, P. Melchior, and A. Oustaloup, *Fractional Order Differentiation and Robust Control Design*, Springer, 2015.
- [2] F. Padula, and A. Visioli, *Advances in Robust Fractional Control*, Springer, 2014.
- [3] S. Das, *Functional Fractional Calculus*, Springer-Verlag Berlin Heidelberg, 2011.
- [4] H. O. Erkol, "Optimal controller design for two wheeled inverted pendulum," *IEEE Access*, vol. 6, pp. 75709-75717, 2018.
- [5] C. Hsu, "Fractional order PID control for reduction of vibration and noise on induction motor," *IEEE Transactions on Magnetics*, vol. 55, no. 11, pp. 1-7, Nov. 2019.
- [6] J. Viola, L. Angel, and J. M. Sebastian, "Design and robust performance evaluation of a fractional order PID controller applied to a DC motor," *IEEE/CAA Journal of Automatica Sinica*, vol. 4, no. 2, pp. 304-314, Apr. 2017.

- [7] W. Zheng, Y. Luo, Y. Pi, and Y. Chen, "Improved frequency-domain design method for the fractional order proportional-integral-derivative controller optimal design: a case study of permanent magnet synchronous motor speed control," *IET Control Theory & Applications*, vol. 12, no. 18, pp. 2478-2487, Dec. 2018.
- [8] B. Hekimoğlu, "Optimal tuning of fractional order PID controller for DC motor speed control via chaotic atom search optimization algorithm," *IEEE Access*, vol. 7, pp. 38100-38114, 2019.
- [9] A. S. Chopade, S. W. Khubalkar, A. S. Junghare, M. V. Aware, and S. Das, "Design and implementation of digital fractional order PID controller using optimal pole-zero approximation method for magnetic levitation system," *IEEE/CAA Journal of Automatica Sinica*, vol. 5, no. 5, pp. 977-989, Sep. 2018.
- [10] J. Viola, and L. Angel, "Delta parallel robotic manipulator tracking control using fractional order controllers," *IEEE Latin America Transactions*, vol. 17, no. 03, pp. 393-400, Mar. 2019.
- [11] J. Viola, and L. Angel, "Tracking control for robotic manipulators using fractional order controllers with computed torque control," *IEEE Latin America Transactions*, vol. 16, no. 7, pp. 1884-1891, Jul. 2018.
- [12] H. P. Ren, X. Wang, J. T. Fan, and O. Kaynak, "Fractional order sliding mode control of a pneumatic position servo system," *Journal of the Franklin Institute*, vol. 356, issue 12, pp. 6160-6174, 2019.
- [13] T. Mahto, and V. Mukherjee, "Fractional order fuzzy PID controller for wind energy-based hybrid power system using quasi-oppositional harmony search algorithm," *IET Generation, Transmission & Distribution*, vol. 11, no. 13, pp. 3299-3309, Sep. 2017.
- [14] A. Asgharnia, R. Shahnaazi, and A. Jamali, "Performance and robustness of optimal fractional fuzzy PID controllers for pitch control of a wind turbine using chaotic optimization algorithms," *ISA Transactions*, vol. 79, pp. 27-44, 2018.
- [15] P. K. Ray, S. R. Paital, A. Mohanty, Y. S. E. Foo, A. Krishnan, H. B. Gooi, and G. A. J. Amaratunga, "A hybrid firefly-swarm optimized fractional order interval type-2 fuzzy PID-PSS for transient stability improvement," *IEEE Transactions on Industry Applications*, vol. 55, no. 6, pp. 6486-6498, Nov.-Dec. 2019.
- [16] J. Z. Shi, "A fractional order general type-2 fuzzy PID controller design algorithm," *IEEE Access*, vol. 8, pp. 52151-52172, 2020.
- [17] S. Xu, G. Sun, Z. Ma, and X. Li, "Fractional-order fuzzy sliding mode control for the deployment of tethered satellite system under input saturation," *IEEE Transactions on Aerospace and Electronic Systems*, vol. 55, no. 2, pp. 747-756, Apr. 2019.
- [18] Z. Yakoub, M. Amairi, M. Chetoui, B. Saidi, and M. Aoun, "Model-free adaptive fractional order control of stable linear time-varying systems," *ISA Transactions*, vol. 67, pp.193-207, 2017.
- [19] H. Wang, L. Hua, Y. Guo, and C. Lu, "Control of Z-axis MEMS gyroscope using adaptive fractional order dynamic sliding mode approach," *IEEE Access*, vol. 7, pp. 133008-133016, 2019.
- [20] F. Chen, and J. Fei, "Fractional order adaptive sliding mode control system of micro gyroscope," *IEEE Access*, vol. 7, pp. 150565-150572, 2019.
- [21] G. Sun, and Z. Ma, "Practical Tracking Control of Linear Motor With Adaptive Fractional Order Terminal Sliding Mode Control," *IEEE/ASME Transactions on Mechatronics*, vol. 22, no. 6, pp. 2643-2653, Dec. 2017.
- [22] P. Gao, G. Zhang, H. Ouyang, and L. Mei, "An adaptive super twisting nonlinear fractional order PID sliding mode control of permanent magnet synchronous motor speed regulation system based on extended state observer," *IEEE Access*, vol. 8, pp. 53498-53510, 2020.
- [23] M. Vahdanipour, and M. Khodabandeh, "Adaptive fractional order sliding mode control for a quadrotor with a varying load," *Aerospace Science and Technology*, vol. 86, pp. 737-747, 2019.
- [24] S. Chen, H. Chiang, T. Liu, and C. Chang, "Precision motion control of permanent magnet linear synchronous motors using adaptive fuzzy fractional-order sliding-mode control," *IEEE/ASME Transactions on Mechatronics*, vol. 24, no. 2, pp. 741-752, April 2019.
- [25] P. Mani, R. Rajan, L. Shanmugam, and Y. H. Joo, "Adaptive Fractional Fuzzy Integral Sliding Mode Control for PMSM Model," *IEEE Transactions on Fuzzy Systems*, vol. 27, no. 8, pp. 1674-1686, Aug. 2019.
- [26] S. A. Moezi, E. Zakeri, and M. Eghtesad, "Optimal adaptive interval type-2 fuzzy fractional-order backstepping sliding mode control method for some classes of nonlinear systems," *ISA Transactions*, vol.93, pp.23-39, 2019.
- [27] Y. Chen, I. Petrás, and D. Xue, "Fractional order control - A tutorial," in *Proc. American Control Conference*, St. Louis, USA, 2009.
- [28] K. J. Astrom, and B. Wittenmark, *Adaptive Control*, Addison-Wesley Publishing Company, 1989.
- [29] B. T. Jevtović, and M. R. Mataušek, "PID Controller Design of TITO System Based On Ideal Decoupler," *Journal of Process Control*, vol. 20, no. 7, pp. 869-876, 2010.
- [30] J.A. Rossiter, B.L. Jones, S. Pope, and J.D. Hedengren, "Evaluation and demonstration of take home laboratory kit," in *Proc. 12th IFAC Symposium on Advances in Control Education (ACE 2019)*, Philadelphia, PA., Jul. 2019.
- [31] J.D. Hedengren, R.A. Martin, J.C. Kantor, N. Reuel, "Temperature control lab for dynamics and control," *AIChE Annual Meeting*, Orlando, FL, Nov. 2019.
- [32] A. Tepljakov, E. Petlenkov, and J. Belikov, "FOMCON: a Matlab toolbox for fractional-order system identification and control," *International Journal of Microelectronics and Computer Science*, vol.2, pp. 51-62, 2011.